nature genetics

MicroRNAs can generate thresholds in target gene expression

Shankar Mukherji[1,7], Margaret S Ebert[2,3,7], Grace X Y Zheng[2,4], John S Tsang[5,8], Phillip A Sharp[2,3] & Alexander van Oudenaarden[2,3,6]

MicroRNAs (miRNAs) are short, highly conserved noncoding RNA molecules that repress gene expression in a sequence-dependent manner. We performed single-cell measurements using quantitative fluorescence microscopy and flow cytometry to monitor a target gene's protein expression in the presence and absence of regulation by miRNA. We find that although the average level of repression is modest, in agreement with previous population-based measurements, the repression among individual cells varies dramatically. In particular, we show that regulation by miRNAs establishes a threshold level of target mRNA below which protein production is highly repressed. Near this threshold, protein expression responds sensitively to target mRNA input, consistent with a mathematical model of molecular titration. These results show that miRNAs can act both as a switch and as a fine-tuner of gene expression.

miRNAs regulate protein synthesis in the cell cytoplasm by promoting target mRNAs' degradation and/or inhibiting their translation. Their importance is suggested by (i) the predictions that each miRNA targets hundreds of genes and that the majority of protein-coding genes are miRNA targets[1–4], (ii) their abundance, with some miRNAs expressed as highly as 50,000 copies per cell[5], and (iii) their sequence conservation, with some miRNAs conserved from sea urchins to humans[6]. miRNAs can regulate a large variety of cellular processes, from differentiation and proliferation to apoptosis[7–11]. miRNAs also confer robustness to systems by stabilizing gene expression during stress and in developmental transitions[12,13].

Despite the evidence for the importance of gene regulation by miRNAs, the typical magnitude of observed repression by miRNAs is relatively small[2,3], with some notable exceptions, such as the switch-like transitions caused by the miRNAs lin-4 and let-7 targeting the heterochronic genes *lin-14* and *lin-41*, respectively, in *Caenorhabditis elegans*[14]. Importantly however, most of the previous studies of regulation by miRNAs in mammalian cells have measured population averages, which often obscure how individual cells respond to signals[15].

In our study, we aimed to complement previous work showing the breadth and importance of gene regulation by miRNA by directly measuring the effects of miRNA on target gene expression in single cells. Through the use of a two-color fluorescent reporter system that allowed us to simultaneously track gene expression in the presence and absence of binding sites for miRNA, we were able to measure both transcription and translation following regulation by miRNA in single mammalian cells. Our single-cell analysis revealed two unexpected features. First, the experiments showed that regulation by miRNA imposes a previously unappreciated nonlinearity relating target transcript abundance to target protein abundance; namely, target protein production is highly repressed below a threshold level of target mRNA production and responds sensitively to transcription above this threshold. Second, there is considerable cell-to-cell variability in the strength of repression in a population of identically prepared cells. Most notably, the fold repression of miRNA targets below the threshold can be far greater than measured for the population average, up to 40-fold greater in our data. Motivated by previous work on protein-protein interactions[16,17] and regulation by bacterial small RNA[18] (sRNA), we employed and experimentally tested a mathematical model to formally describe the biochemical interactions comprising the miRNA regulatory system. The model suggested the importance of molecular titration in generating the sensitive response to transcription above the threshold. In this picture, as target abundance increases, target mRNAs titrate away the pool of miRNAs available for repression; the sharpness of the switch from full repression to escape from miRNA repression depends on the strength of the interaction between the miRNA and its target as well as the relative abundance of each.

[1]Harvard–Massachusetts Institute of Technology Division of Health Sciences and Technology, Massachusetts Institute of Technology, Cambridge, Massachusetts, USA. [2]Koch Institute for Integrative Cancer Research, Massachusetts Institute of Technology, Cambridge, Massachusetts, USA. [3]Department of Biology, Massachusetts Institute of Technology, Cambridge, Massachusetts, USA. [4]Computational and Systems Biology Graduate Program, Massachusetts Institute of Technology, Cambridge, Massachusetts, USA. [5]Graduate Program in Biophysics, Harvard University, Cambridge, Massachusetts, USA. [6]Department of Physics, Massachusetts Institute of Technology, Cambridge, Massachusetts, USA. [7]These authors contributed equally to this work. [8]Present addresses: Howard Hughes Medical Institute and FAS Center for Systems Biology, Harvard University, Cambridge, Massachusetts, USA (S.M.); Howard Hughes Medical Institute and Laboratory of Neural Circuits and Behavior, The Rockefeller University, New York, New York, USA (M.S.E.); Howard Hughes Medical Institute and Program in Epithelial Biology, Stanford School of Medicine, Stanford, California, USA (G.X.Y.Z.); and Systems Genomics and Bioinformatics Unit, Laboratory of Systems Biology, National Institute of Allergy and Infectious Diseases, US National Institutes of Health, Bethesda, Maryland, USA (J.S.T.). Correspondence should be addressed to A.v.O. (avano@mit.edu).

Received 24 November 2010; accepted 14 July 2011; published online 21 August 2011; doi:10.1038/ng.905

RESULTS

Microscopy reveals miRNA-mediated gene expression thresholds

To assay for miRNA activity in single mammalian cells, we constructed a two-color fluorescent reporter system that permits simultaneous monitoring of protein levels in the presence and absence of regulation by miRNA (**Fig. 1a**). The construct consists of a bidirectional Tet-inducible promoter driving two genes expressing the fluorescent proteins mCherry and enhanced yellow fluorescent protein (eYFP) tagged with nuclear localization sequences. The 3′ untranslated region (UTR) of mCherry is engineered to contain *N* binding sites for miRNA regulation. In the first set of experiments, the inserted sites are recognized by miR-20, which is expressed endogenously in HeLa cells along with its seed family members miR-17-5p and miR-106b. The 3′ UTR of eYFP is left unchanged so that it can serve as a reporter of the transcriptional activity in a single cell.

We constructed cell lines that stably expressed the fluorescent reporter construct with either a single bulged miR-20 binding site or no site in the mCherry 3′ UTR. We measured the levels of eYFP and mCherry in single cells using quantitative fluorescence microscopy. Arranging individual cells according to their eYFP expression level, we observed that cells whose mCherry 3′ UTR lacked miRNA binding sites had a concomitant increase in mCherry expression (**Fig. 1b**). This indicates that in the absence of miRNA targeting of the mCherry mRNA, the level of expression of eYFP is proportional to the level of expression of mCherry. However, in cells with one miR-20 site in the mCherry 3′ UTR, the eYFP fluorescence initially increases with virtually no corresponding increase in mCherry expression level (**Fig. 1c**). To capture this behavior quantitatively, we measured the joint distributions of mCherry and eYFP levels in single cells, binned the single-cell data according to their eYFP levels and calculated the mean mCherry level in each eYFP bin (Online Methods and **Supplementary Fig. 1**). We refer to this binned joint distribution as the 'transfer function'. As suggested by the representative single cells shown in **Figure 1b**, the transfer function shows a threshold-linear behavior in which the mCherry level, which represents the target protein production, does not appreciably rise until a threshold level of eYFP is exceeded.

A molecular titration model for thresholding

We developed a mathematical model of miRNA-mediated regulation that could reproduce the nonlinearity in the above transfer function (**Fig. 2**). This model (**Fig. 2a**) is inspired by previous models[16] used to describe protein-protein titration[17] and sRNA regulation in bacterial systems[18]. It describes the concentration of free target mRNA (r) subject to regulation by miRNA (m) as a function of bare transcriptional activity in the absence of regulation by miRNA (r_0). We assume that only r can be translated into protein. Experimentally, we expect the mCherry signal to be proportional to the concentration of r and the eYFP signal to be proportional to the concentration of r_0. The core of the model involves the binding of r to m to form an mRNA-miRNA complex r^* and the release of m from the complex back into the pool of active miRNA molecules either with or without the accompanying destruction of r. We assume that the total amount of miRNA is constant. Indeed, we observed no decrease in the miR-20 level beyond the level of experimental uncertainty as a function of eYFP (**Supplementary Fig. 2**). The qualitative shape of the transfer functions generated by the model depends on two key lumped parameters. The first parameter λ, which behaves like a dissociation constant, governs the sharpness of the threshold (**Fig. 2b**). On a log-log plot relating r to r_0 (**Fig. 2d**), the increased sharpness manifests itself as a slope (which we refer to as the logarithmic gain) greater than 1, marking a sensitive transition connecting the branches of the transfer function of slope 1 that indicate little protein expression (below the transition) and nearly maximal protein production (above the transition). λ is inversely proportional to the rate constant at which miRNA binds the target mRNA (k_{on}); as k_{on} increases, while holding the miRNA-target mRNA unbinding rate constant k_{off} fixed, λ decreases and thus sharpens the transition. The threshold constant θ plays a role in the placement of the threshold and also in the sharpness of the transition between the threshold and escape regimes (**Fig. 2c**). θ is proportional to the concentration of free miRNA available within the cell; as the total concentration of free miRNAs increases, θ increases and pushes the threshold to higher values of r_0 (**Fig. 2e**). We also considered a model that accounted for competition from the population of endogenous miRNA targets and found that including a pool of competing miRNA targets results simply in rescaling the θ and λ parameters characterizing the single-target model (**Supplementary Note**).

The mathematical model thus suggests experiments that could be performed to modulate the thresholds generated by miRNA-mediated regulation. As our stable Tet-On HeLa cell lines could not achieve high enough levels of reporter expression to capture the complete sensitive transition to escape from miRNA-mediated repression, we performed subsequent experiments by transiently transfecting Tet-On HeLa cells with reporter constructs and measuring fluorescence using flow cytometry to increase the number of cells in the datasets. As with the quantitative fluorescence microscopy, we restricted our analysis to cells whose fluorescence was above the cellular autofluorescence with at least, and in most cases greater than, 95% confidence.

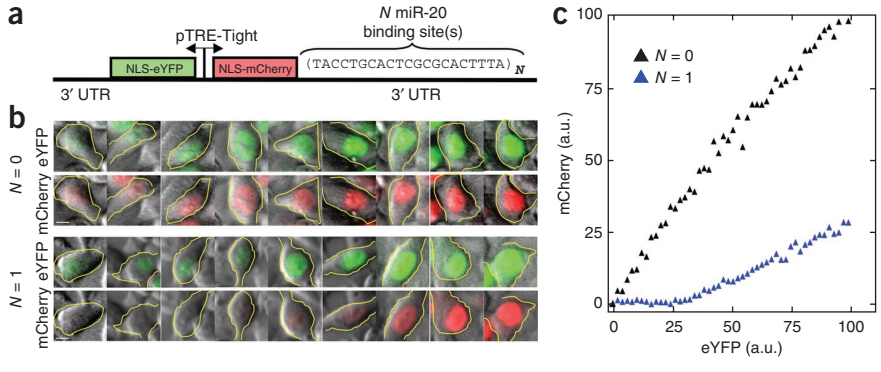

Figure 1 Quantitative fluorescence microscopy reveals the miRNA-mediated gene expression threshold. (**a**) The two-color fluorescent reporter construct consists of a bidirectional Tet promoter that co-regulates enhanced yellow fluorescent protein (eYFP) and mCherry. Each fluorescent protein is tagged with a nuclear localization sequence (NLS) to aid in image analysis. The 3′ UTR of the mCherry gene is engineered to contain *N* binding sites for the miRNA miR-20. (**b**) Sample fluorescence microscopy data from representative single cells stably expressing eYFP and mCherry both in the presence and absence of regulation of mCherry by miR-20. The cells are arranged according to eYFP intensity. Scale bars, 5 μm. (**c**) Transfer function relating eYFP to mCherry generated by binning according to eYFP intensity and plotting the mean mCherry in each bin (a.u: arbitrary units). **Supplementary Figure 1** depicts a schematic of how the binning was performed on similarly structured flow cytometry data.

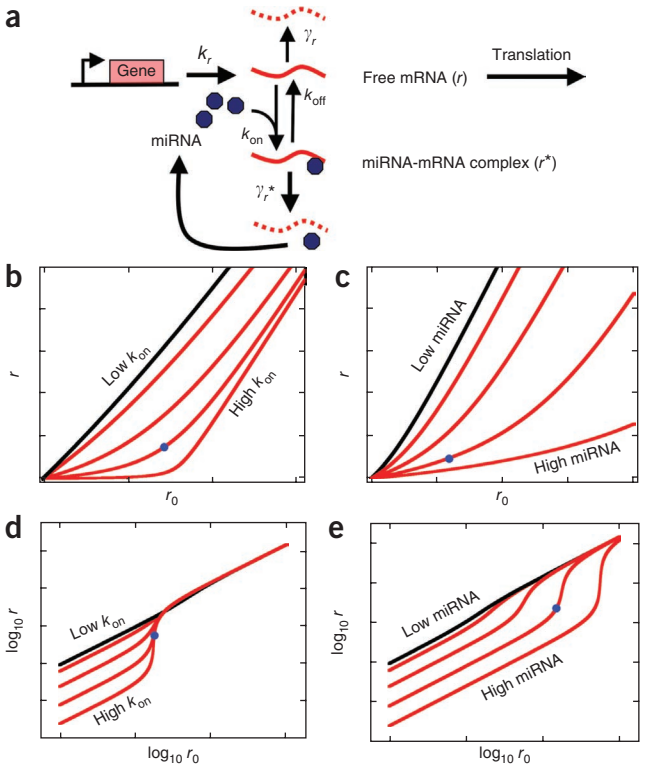

Figure 2 Biochemical model of miRNA-mediated gene regulation. (**a**) The model describes the steady-state level of mRNA free to be translated (r), which we experimentally observed as the mCherry signal, subject to regulation by miRNA (m) as a function of bare transcriptional activity in the absence of regulation by miRNA (r_0), which we experimentally observed as eYFP. The target mRNA is transcribed (rate constant k_r) and intrinsically decays (rate constant γ_r). miRNA and mRNA bind (rate constant k_{on}) to form a complex (r^*). The bound miRNA can reenter the pool of active miRNA either by unbinding the target mRNA (rate constant k_{off}) or destroying the mRNA (rate constant γ_{r^*}). The steady-state solution for r allows us to combine these microscopic parameters into two lumped parameters that govern the shape of the transfer function: λ, the effective dissociation constant characterizing the strength of the miRNA-mRNA interaction, and θ, which is proportional to the concentration of miRNA that acts on the target mRNA. (**b**) Steady-state solutions for r as a function of r_0 for various values of k_{on}; increasing k_{on} decreases λ. (**c**) Steady-state solutions for r as a function of r_0 for various values of miRNA_{total}; increasing miRNA_{total} increases θ. (**d**,**e**) The same solutions as in **b** and **c** except depicted on log-log axes. The slope of the log-log curve is known as the logarithmic gain. Notably, thresholds in the linear representation appear as segments with logarithmic gain greater than 1 in the log-log representation. Increasing k_{on} increases the maximum logarithmic gain but does not change its position along the r_0 axis, whereas increasing miRNA_{total} increases the maximum logarithmic gain and shifts it to higher levels of r_0. Blue dots in **b**–**e** are guides to the eye to facilitate comparison between linear and logarithmic plots.

Sharpening the threshold by adding miRNA binding sites

To sharpen the thresholds by increasing k_{on}, we increased the number of miRNA binding sites N in the 3′ UTR of mCherry. The maximum logarithmic gain increased from approximately 1 when $N = 1$ to 1.8 when $N = 7$ (**Fig. 3a**); as expected from the model, the effect was stronger when going from 1 to 4 binding sites than from 4 to 7 sites. We were also able to recapitulate a similar transfer function with $N = 7$ in the 3′ UTR of eYFP, thus isolating the effect to miR-20–mediated regulation rather than any property intrinsic to the mCherry reporter (**Supplementary Fig. 3**). Notably, unlike previous studies of bacterial sRNA[18], we could also directly test the importance of titration in the generation of the threshold by using miR-20 binding sites that are perfectly complementary to endogenous miR-20, thus converting the interaction between target and miRNA into a catalytic, RNA interference–type repression. When the multiple miR-20 bulged binding sites were replaced by a single perfectly complementary binding site that yields the same maximum repression as $N = 7$ bulged sites, we did not observe gene expression thresholding (**Fig. 3a**, gray points).

To measure the fold repression as a function of target expression level, we measured for individual cells the transfer function in the absence of miR-20 binding sites and calculated the ratio of this control transfer function to transfer functions in the presence of one, four and seven miR-20 sites (**Fig. 3b**). As expected from **Figure 3a**, increasing the number of binding sites increased the fold repression at lower eYFP levels, from just over twofold repression with a single miR-20 site to approximately tenfold repression with seven miR-20 sites, while not significantly changing the fold repression at high eYFP levels (**Fig. 3b**). Seen this way, we show that rather than being only a subtle

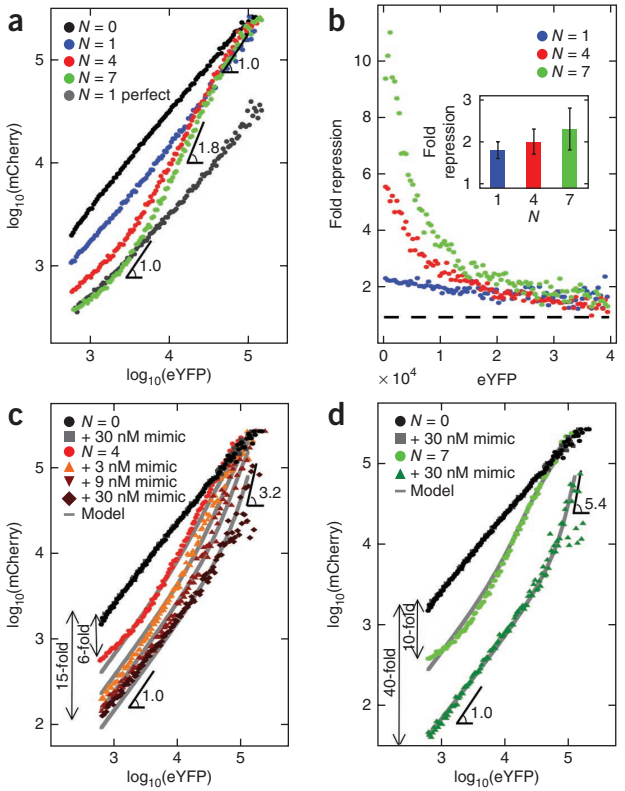

Figure 3 Modulating the threshold. (**a**) Log-log transfer functions for $N = 0$, 1, 4 and 7. We can abolish the threshold by using an miR-20 binding site that is perfectly complementary to miR-20. (**b**) Ratio of $N = 0$ transfer function to $N = 1$, 4 and 7 transfer functions, depicting the fold repression as a function of eYFP expression. Inset depicts the average fold repression as a function of N. Using the flow cytometry data from **a**, we computed the ratio of the mean eYFP level to the mean mCherry level for $N = 1$, 4, and 7. We then normalized this ratio by the mean eYFP to mean mCherry ratio for $N = 0$; we refer to this normalized ratio as the fold repression. We estimated the error bars by bootstrap sampling of the flow cytometry data. (**c**,**d**) Effects of titrating defined amounts of miR-20 mimic siRNA on the transfer function for $N = 4$ (**c**) and $N = 7$ (**d**). In **a**, **c** and **d** the angle symbol followed by a number denotes the value of the logarithmic gain, either minimum (when gain = 1) or maximum (when gain >1).

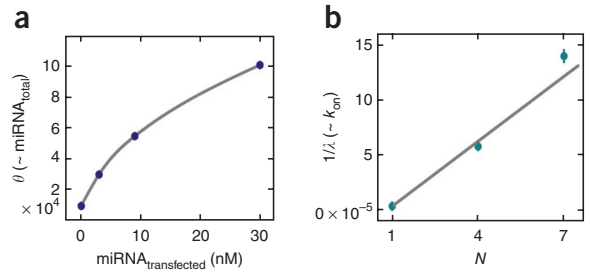

Figure 4 Comparison to model. (**a**,**b**) Following simultaneous fitting of all transfer function data to the quantitative model, the fitting parameter θ, which is proportional to the total amount of active miR-20 in the cell, is plotted against the amount of miR-20 mimic transfected (**a**), and $1/\lambda$, which is proportional to the rate constant of mCherry–miR-20 association, is plotted against N (**b**).

effect as suggested by population-based averages, which in this case would result in at most 2.5-fold repression with seven binding sites (**Fig. 3b**, inset), regulation by miR-20 can exert very strong repression of protein production at low target transcript levels. Moreover, the boundary of the regime of strongest repression is marked by a threshold level of transcription. Shifting this threshold to lower or higher target mRNA levels by changing miRNA levels or the number of binding sites can be of functional importance.

Shifting the threshold by modulating miR-20 abundance

Consistent with the model, the threshold can be shifted to either higher or lower eYFP levels by transfecting either miR-20 mimic oligonucleotides (small interfering RNAs (siRNAs)) or miRNA sponges that inhibit miR-20 activity[19] (**Fig. 3c**,**d** and **Supplementary Fig. 4**). Increasing the level of miRNA increased the fold repression below the threshold, increased the mRNA level needed to reach the threshold and sharpened the transition. In the extreme case of seven miR-20 binding sites with 30 nM miR-20 mimic transfected (**Fig. 3d**), miRNA-mediated repression was ~40-fold greater compared to a target with no miRNA binding site, the threshold was shifted to a tenfold higher eYFP level, and the transition between repressed and unrepressed expression was quite sharp, with a maximum logarithmic gain of ~5.4 (**Fig. 3d**), compared to ~1.8 without the transfected miR-20 mimic (endogenous levels) (**Fig. 3a**). To quantitatively compare the data to the model, we simultaneously fit all the datasets, holding λ constant across the fits for particular values of the constants N and θ for a particular amount of transfected siRNA mimic. Notably, the fit parameter θ, which is proportional to the concentration of miRNA available for target repression, increased with increasing siRNA mimic (**Fig. 4a**) but in a saturable fashion, whereas $1/\lambda$ increased linearly with N (**Fig. 4b**). The saturation suggests that the amount of transfected siRNA mimic entering functional complexes and thus available for target repression is limited, perhaps by entry into the cytoplasm and/or loading into Argonaute protein complexes.

Measuring gene expression thresholds in natural contexts

In order to test the generality of these findings, that the strength of repression of a miRNA target depends strongly on the relative amounts of the miRNA and its target, we sought to recapitulate the results in more physiological settings. First, we tested whether similarly sensitive transitions would be observed when the reporter construct incorporated naturally occurring miRNA binding sequences by fusing the 3′ UTRs of the oncogene *HMGA2* and the major GABA transporter gene *SLC6A1* to the mCherry reporter and performing dual-color flow cytometry. The *HMGA2* 3′ UTR contains seven binding sites for the miRNA family let-7, which is moderately expressed in HeLa cells, whereas *SLC6A1* contains three binding sites for the neuronal miRNA miR-218, which we supplied exogenously. The experiments showed that we could indeed observe sensitive transitions with these constructs (**Fig. 5a**,**b**). In addition, for *HMGA2*, we increased the threshold incrementally by transfecting higher doses of let-7 siRNA mimic (**Fig. 5a**).

Finally, we used a standard dual luciferase assay (Online Methods and **Supplementary Fig. 5**) to measure target expression in mouse embryonic stem (ES) cells using only their endogenous pool of miRNA to retain physiological relevance. Here we measured a transfer function complementary to that in the experiments with HeLa cells: the mRNA target level remained fixed while the miRNA concentration varied. To test varying miRNA concentrations in ES cells, we exploited the fact that different miRNA species are present at different abundances[20]. Finally, to gauge the strength of miRNA repression, we normalized target expression in wild-type ES cells to target expression in ES cells that lack the enzyme Dicer (Dcr) and thus contain no miRNAs. We observed a similar threshold-linear behavior as with the miR-20 reporter in Tet-On HeLa cells, except that the behavior reflected the level of miRNAs (**Supplementary Fig. 5**): at high miRNA abundances, repression was fivefold, but it decreased with miRNA abundance until at the lowest miRNA levels, target expression in wild-type cells was virtually indistinguishable from that in the miRNA-free Dcr$^{-/-}$ cells.

The threshold in regulation by miRNA is determined by the level of the miRNA and by the number and affinity of the target sites. Taking the case described above for regulation by endogenous miR-20 in HeLa cells, the threshold transition starts at approximately 60 target mRNAs per cell with seven typical sites in the 3′ UTR at an endogenous level of approximately 2,000 miR-20 molecules per cell (**Supplementary Figs. 2** and **6**). Many of these miRNAs as miRNA ribonucleoprotein complexes could be bound to the endogenous miR-20 target mRNAs in the cell, leaving a limited pool for binding

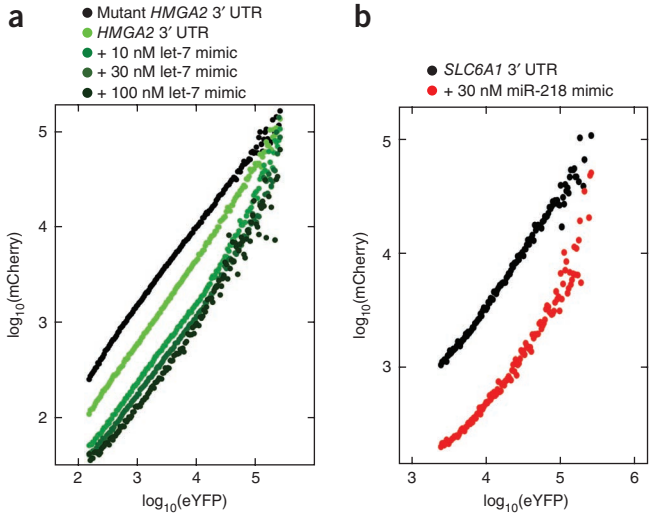

Figure 5 Thresholding in endogenous 3′ UTRs. (**a**) We fused to mCherry the 3′ UTR of *HMGA2* or a version with the seven let-7 seed matches mutated. The reporters were cotransfected with varying concentrations of let-7b mimic. Cells were assayed by flow cytometry 48 h after transfection. (**b**) We fused the 3′ UTR of *SLC6A1*, which contains three seed matches for miR-218, to mCherry. The reporter was transfected with or without miR-218 mimic. Cells were assayed by flow cytometry 48 h after transfection.

to the reporter mRNAs. Because these experiments were done at steady-state conditions, this suggests that the miRNA system probably has limited capacity to accommodate increases in target populations. These results are consistent with our ability to strongly suppress miR-20 regulation of the target reporter by adding high levels of miR-20 target sites in the form of an exogenous sponge inhibitor[19] (**Supplementary Fig. 4**). The sponge phenomenon has been observed in multiple mammalian and non-mammalian organisms, indicating its generality in miRNA regulation[21].

DISCUSSION

Our analysis of miRNA-mediated gene regulation at high target expression levels is consistent with previous population-based results, but measuring single cells offers a level of detail inaccessible to bulk assays. The detailed picture, which revealed a sensitive response of protein production to transcriptional activity bounded by strong repression at low target mRNA levels and weak repression at high target mRNA levels, may have important implications for miRNA-mediated regulation. There has been disparity between the concept of miRNAs as switches, exemplified by the *lin-14* developmental switch in *C. elegans*, where there is a high degree of repression by the miRNA lin-4, compared to many observations of miRNA-mediated regulation in mammalian cells, where they are best considered as fine-tuners of gene expression. These results show that for some miRNA-target interactions, the miRNA behaves both as a switch, in the target expression regime below the threshold, and as a fine-tuner, in the sensitive transition between the threshold and the minimal repression regime at high mRNA levels.

The multi-site targets that we assayed are relevant to natural target genes because, though most target genes have only one conserved binding site for a given miRNA seed family, the majority of targets have sites for multiple miRNA families, with an average of more than four total conserved sites per 3′ UTR and many more poorly conserved sites[4]. This is further exemplified by the above results, with targets containing natural miRNA sites from *HMGA2* and *SLC6A1*. In addition, we observed target reporter repression predominantly at the level of mRNA degradation (**Supplementary Fig. 6d**), as has been observed in genome-wide measurements of natural targets[22].

Our data and model suggest that the difference in repression between high and low target expression levels need not be inconsistent with the recently reported independence of the strength of repression of different target genes from their expression level[22]. Our results suggest that if the target pool of an miRNA is below the saturation regime, then all targets of a given affinity for the miRNA will be repressed to the same degree regardless of expression level. But if the target pool size grows, as it does when we introduce our reporter construct, then it is possible to saturate the pool of miRNAs. Our data and model are consistent with the dampening of the fold repression as target expression goes from low to high levels being caused by titration of the available cognate miRNA. This agrees with the observation that when the target contains a perfectly complementary site invoking an RNA interference–type catalytic repressive mechanism, the threshold is abolished. Here there should be little stable titration of available miRNA. When a given miRNA target's abundance rises appreciably enough to titrate the miRNA, as we tested using sponge constructs, all the targets of that miRNA, not only the mCherry reporter, should experience derepression. These titration effects could also explain results from retrospective bioinformatic studies showing that an miRNA's overall target abundance negatively correlates with the miRNA's average repressive strength[23]. Mathematical modeling suggests that the pool of target mRNAs limits the ability of free miRNAs to bind to and repress additional targets (**Supplementary Note**). In this regard, natural noncoding RNAs such as, potentially, pseudogene RNAs with UTR sequences matching those of protein-coding target genes[24] would also participate in this pool of competing molecules.

Gene expression thresholding may be an important feature of cell fate decisions. During a developmental transition where a tissue-specific miRNA is upregulated and its pool of target genes are downregulated, a trend that has been reported in fruitflies and in mammals[25,26], the miRNA's effective concentration and therefore its potency could greatly increase. A target gene whose protein exerts its function at concentrations only above the threshold should have a switch-like response. Switch-like derepression through molecular titration of miRNA could also enhance interactions within genetic networks. It has been shown that miRNAs often coordinately regulate targets that function together in pathways and protein complexes[27]. If the effect of the miRNA that targets such a gene network were sensitively switched off through titration, then the gene network could rapidly switch 'on' in a coordinated manner.

METHODS

Methods and any associated references are available in the online version of the paper at http://www.nature.com/naturegenetics/.

Note: Supplementary information is available on the Nature Genetics website.

ACKNOWLEDGMENTS

This work was supported by the US National Institutes of Health (NIH) Director's Pioneer Award to A.v.O. (1DP1OD003936) and the NIH–National Cancer Institute (NCI) Physical Sciences Oncology Center at the Massachusetts Institute of Technology (U54CA143874); and by US Public Health Service grants R01-CA133404 , R01-GM34277 from the NIH, PO1-CA42063 from the NCI (to P.A.S.) and partially by Cancer Center Support (core) grant P30-CA14051 from the NCI. M.S.E. was supported by a Howard Hughes Medical Institute Predoctoral Fellowship and a Paul and Cleo Schimmel Scholarship. G.X.Y.Z. and J.S.T. were partially supported by Natural Sciences and Engineering Research Council of Canada Post Graduate Scholarships. We thank G. Neuert for help with cloning the reporter genes, Koch Institute flow cytometry staff for training and cell sorting and D. Bartel for helpful discussions.

AUTHOR CONTRIBUTIONS

M.S.E., J.S.T., P.A.S. and A.v.O. conceived the project. M.S.E., S.M. and G.X.Y.Z. performed the experiments. S.M. and M.S.E. processed the data and constructed the model, and S.M. quantitatively analyzed the model. S.M., M.S.E., A.v.O. and P.A.S. interpreted the results and wrote the paper.

COMPETING FINANCIAL INTERESTS

The authors declare no competing financial interests.

Published online at http://www.nature.com/naturegenetics/.
Reprints and permissions information is available online at http://www.nature.com/reprints/index.html.

1. Lewis, B.P., Burge, C.B. & Bartel, D.P. Conserved seed pairing, often flanked by adenosines, indicates that thousands of human genes are microRNA targets. *Cell* **120**, 15–20 (2005).
2. Selbach, M. *et al.* Widespread changes in protein synthesis induced by microRNAs. *Nature* **455**, 58–63 (2008).
3. Baek, D. *et al.* The impact of microRNAs on protein output. *Nature* **455**, 64–71 (2008).
4. Friedman, R.C., Farh, K.K., Burge, C.B. & Bartel, D.P. Most mammalian mRNAs are conserved targets of microRNAs. *Genome Res.* **19**, 92–105 (2009).
5. Lim, L.P. *et al.* The microRNAs of *Caenorhabditis elegans*. *Genes Dev.* **17**, 991–1008 (2003).
6. Grimson, A. *et al.* Early origins and evolution of microRNAs and Piwi-interacting RNAs in animals. *Nature* **455**, 1193–1197 (2008).
7. Yi, R., Poy, M.N., Stoffel, M. & Fuchs, E. A skin microRNA promotes differentiation by repressing 'stemness'. *Nature* **452**, 225–229 (2008).
8. Sluijter, J.P.G. *et al.* MicroRNA-1 and -499 regulate differentiation and proliferation in human-derived cardiomyocyte progenitor cells. *Arterioscler. Thromb. Vasc. Biol.* **30**, 859–868 (2010).
9. Cimmino, A. *et al.* miR-15 and miR-16 induce apoptosis by targeting Bcl2. *Proc. Natl. Acad. Sci. USA* **102**, 13944–13949 (2005).

10. Li, X. & Carthew, R.W. A microRNA mediates EGF receptor signaling and promotes photoreceptor differentiation in the *Drosophila* eye. *Cell* **123**, 1267–1277 (2005).
11. Bernstein, E. *et al.* Dicer is essential for mouse development. *Nat. Genet.* **35**, 215–217 (2003).
12. Li, X., Cassidy, J.J., Reinke, C.A., Fischboeck, S. & Carthew, R.W. A microRNA imparts robustness against environmental fluctuation during development. *Cell* **137**, 273–282 (2009).
13. Li, Y., Wang, F., Lee, J.A. & Gao, F.B. MicroRNA-9a ensures the precise specification of sensory organ precursors in *Drosophila*. *Genes Dev.* **20**, 2793–2805 (2006).
14. Bagga, S. *et al.* Regulation by let-7 and lin-4 miRNAs results in target mRNA degradation. *Cell* **122**, 553–563 (2005).
15. Raj, A. & van Oudenaarden, A. Nature, nurture, or chance: stochastic gene expression and its consequences. *Cell* **135**, 216–226 (2008).
16. Elf, J., Paulsson, J., Berg, O.G. & Ehrenberg, M. Near-critical phenomena in intracellular metabolite pools. *Biophys. J.* **84**, 154–170 (2003).
17. Buchler, N. & Louis, M. Molecular titration and ultrasensitivity in regulatory networks. *J. Mol. Biol.* **384**, 1106–1119 (2008).
18. Levine, E., Zhang, Z., Kuhlman, T. & Hwa, T. Quantitative characteristics of gene regulation by small RNA. *PLoS Biol.* **5**, e229 (2007).
19. Ebert, M.S., Neilson, J.R. & Sharp, P.A. MicroRNA sponges: competitive inhibitors of small RNAs in mammalian cells. *Nat. Methods* **4**, 721–726 (2007).
20. Calabrese, J.M., Seila, A.C., Yeo, G.W. & Sharp, P.A. RNA sequence analysis defines Dicer's role in mouse embryonic stem cells. *Proc. Natl. Acad. Sci. USA* **104**, 18097–18102 (2007).
21. Ebert, M.S. & Sharp, P.A. MicroRNA sponges: progress and possibilities. *RNA* **16**, 2043–2050 (2010).
22. Guo, H., Ingolia, N.T., Weissman, J.S. & Bartel, D.P. Mammalian microRNAs predominantly act to decrease target mRNA levels. *Nature* **466**, 835–840 (2010).
23. Arvey, A., Larsson, E., Sander, C., Leslie, C.S. & Marks, D.S. Target mRNA abundance dilutes microRNA and siRNA activity. *Mol. Syst. Biol.* **6**, 363 (2010).
24. Poliseno, L. *et al.* A coding-independent function of gene and pseudogene mRNAs regulates tumour biology. *Nature* **465**, 1033–1038 (2010).
25. Stark, A., Brennecke, J., Bushati, N., Russell, R.B. & Cohen, S.M. Animal microRNAs confer robustness to gene expression and have a significant impact on 3′ UTR evolution. *Cell* **123**, 1133–1146 (2005).
26. Farh, K.K. *et al.* The widespread impact of mammalian microRNAs on mRNA repression and evolution. *Science* **310**, 1817–1821 (2005).
27. Tsang, J.S., Ebert, M.S. & van Oudenaarden, A. Genome-wide dissection of microRNA functions and cotargeting networks using gene set signatures. *Mol. Cell* **38**, 140–153 (2010).

ONLINE METHODS

Reporter plasmid construction. Fluorescent reporters were cloned into pTRE-Tight-BI (Clontech). NLS sequences (ATGGGCCCTAAAAAGAAGCGTA AAGTC) were appended to the N terminus of the eYFP and mCherry open reading frames (Clontech) by PCR. The NLS-eYFP was inserted with EcoRI and NdeI. The NLS-mCherry was inserted with BamHI and ClaI. Regulatory elements were placed into the eYFP 3′ UTR with NdeI and XbaI and into the mCherry 3′ UTR with ClaI and EcoRV. The $N = 1$ bulged miR-20 binding site (TACCTGCACTCGCGCACTTTA) was appended by PCR. The $N = 4$ and $N = 7$ miR-20 sites, separated by CCGG spacers, were PCR amplified from miR-20 sponge constructs (Ebert 2007). All constructs were sequence confirmed. *HMGA2* wild-type and seed-mutant 3′ UTRs[28] were a gift from C. Mayr from the David Bartel lab at MIT. The *SLC6A1* 3′ UTR fragment (nt 703–2,041) was PCR amplified from human genomic DNA. For a list of primers used in plasmid construction, please refer to **Supplementary Table 1**.

Generation of stable lines. Reporter plasmids were linearized with AseI and cotransfected at a 20:1 ratio with linear puromycin marker (Clontech). Transfected cells were selected in 2.5 μg/ml puromycin with 200 μg/ml G418. Individual eYFP-positive colonies were isolated, grown and sorted for eYFP positivity upon dox induction (MoFlo, DAKO-Cytomation).

Fluorescence microscopy. Cells were plated on glass-bottomed Nunc chambers (#1) and induced with dox for 4 days to ensure steady state reporter expression levels; cell confluency was ~90%. This level of confluency was held constant between different constructs in any given experiment. Roughly 2,500 cells were imaged in a Nikon TEI-2000 inverted fluorescence microscope with a Princeton Instruments Pixis back-cooled CCD camera. Images were processed using custom software in MATLAB. Briefly, following subtraction of camera background and any cellular autofluorescence, pixel values in both eYFP and mCherry channels corresponding to cells expressing the construct were extracted. The single-cell data were then binned along the eYFP axis. **Figure 1c** reports the results of this binning procedure. In order to ensure that our measurements were within the dynamic range of our instruments, we only included data with a 95% confidence level above the autofluorescent background for analysis in both the fluorescence microscopy and flow cytometry experiments.

Transient transfection. Tet-On HeLa cells (Clontech) below passage 10 were plated in G418 (Gibco) 200 μg/ml and doxycycline (Sigma) 1 μg/ml media in 12-well dishes the day before transfection. Reporter plasmids were diluted 1:50 in pUC18b carrier plasmid (QIAGEN HiSpeed maxipreps) and mixed with DreamFect Gold (Oz Biosciences), 8 μl reagent and 2 μg DNA per well. miR-20a, let-7b and miR-218 mimics (Dharmacon) were cotransfected at the indicated concentrations. For U6 sponge assays, reporter plasmids were diluted 1:50 in sponge plasmid. Media was changed 24 h after transfection. Assays were performed 48 h after transfection. Reporter transfections were also performed with Lipofectamine 2000 (Invitrogen), with the same results.

Flow cytometry. Cells were run on LSRII analyzer (Becton Dickinson) with FACSDiva software. As above, cell confluency was ~90%. This level of confluency was held constant between different constructs in any given experiment. The raw FACS data were analyzed with FlowJo to gate cells according to their forward (FSC-A) and side (SSC-A) scatter profiles; specifically, we chose cells near the peak of the (FSC-A, SSC-A) joint distribution. Untransfected cells were used to characterize the cellular autofluorescence in the LSRII analyzer from which we obtained the mean and standard deviation of the autofluorescence distribution. The mean autofluorescence plus twice the standard deviation were subtracted from each cell's eYFP and mCherry fluorescence values. Following background subtraction, cells with eYFP fluorescence levels less than 0 (meaning, indistinguishable from background) were excluded from further analysis. The single-cell data were then binned in the same manner as described above.

Fluorescence-activated cell sorting. Cells transfected with the $N = 0$ or $N = 7$ reporter were sorted 48 h after transfection into low and high fractions using a MoFlo high-speed sorting instrument (DAKO-Cytomation). Cell pellets were washed and snap frozen before RNA isolation.

RT-PCR. Total RNA was harvested using RNeasy Micro Plus kit with the protocol modified for inclusion of small RNAs (QIAGEN). RNA was treated with DNaseI (Ambion) and reverse transcribed with oligo-dT primer using MMLV RTase (Ambion). Quantitative PCR for mCherry and eYFP was performed in triplicate reactions using SYBRGreen mix (Applied Biosystems) run on an Applied Biosystems 7500 Real-Time PCR instrument. Single-stranded DNA standards spiked into untransfected cell complementary DNAs were used for estimation of mCherry mRNAs per cell. miR-20 was measured with miScript RT-PCR assay (QIAGEN) in quadruplicate reactions using miR-31 and small nucleolar RNA as controls.

Small RNA blot. Total RNA was extracted from transfected cells with TRIzol (Invitrogen). Twenty-four micrograms of total RNA was run on 12% polyacrylamide gel (UreaGel system, National Diagnostics), with miR-20 mimic as a standard, spiked into yeast sheared total RNA (Ambion). The blot was probed for miR-20a and $tRNA_{gln}$ as a loading control. Quantitation of bands was performed with ImageJ.

Mouse ES cell luciferase assays. Reporters were constructed by insertion of two bulged binding sites into the 3′ UTR of CMV Renilla luciferase. Cells were transfected in triplicate in 24-well plates with 2 μl Lipofectamine 2000 (Invitrogen), 0.01 μg of CMV-Renilla plasmid, 0.1 μg of pGL3 (Promega) and 0.69 μg of pWS (carrier plasmid). Cells were lysed and assayed 24 h after transfection by Dual Luciferase reporter assay (Promega) using a Glomax 20/20 luminometer (Promega).

28. Mayr, C., Hemann, M.T. & Bartel, D.P. Disrupting the pairing between let-7 and Hmga2 enhances oncogenic transformation. *Science* **315**, 1576–1579 (2007).